Available online at www.sciencedirect.com
SCIENCE DIRECT
Journal of Catalysis 232 (2005) 402–410
JOURNAL OF CATALYSIS
www.elsevier.com/locate/jcat

# Carbon-supported Pt–Sn electrocatalysts for the anodic oxidation of $H_2$, CO, and $H_2$/CO mixtures. Part II: The structure–activity relationship

M. Arenz [1], V. Stamenkovic, B.B. Blizanac, K.J. Mayrhofer, N.M. Markovic, P.N. Ross *

*Materials Science Division, Lawrence Berkeley National Laboratory, University of California, Berkeley, CA 94720, USA*

Received 29 November 2004; revised 9 March 2005; accepted 15 March 2005

Available online 10 May 2005

**Abstract**

The catalytic activity of three different carbon-supported Pt–Sn catalysts for the anodic oxidation of hydrogen, carbon monoxide, and $H_2$/CO mixtures is correlated with the bimetallic microstructure established in Part I [V. Radmilovic, T.J. Richardson, S.J. Chen, P.N. Ross, Jr., J. Catal. 232 (2005) 199–209] of this study. These catalysts differ primarily by having differing amounts of Pt, $Pt_3Sn$, PtSn, and $SnO_2$ phase nanoparticles distributed on the carbon support. Further surface chemical characterization of the $Pt_3Sn$ nanoparticles is provided by comparison of in situ vibrational spectra of CO adsorbed on the nanoparticles with CO adsorbed on $Pt_3Sn(hkl)$ surfaces [V. Stamenkovic, M. Arenz, B.B. Blizanac, K.J.J. Mayrhofer, P.N. Ross, N.M. Markovic, Surf. Sci. 576 (2005) 145–157; V.R. Stamenkovic, M. Arenz, C.A, Lucas, M.E. Gallagher, P.N. Ross, N.M. Markovic, J. Am. Chem. Soc. 125 (2003) 2736–2745]. Qualitative measures of CO oxidation activity were also obtained from the FTIR spectra for the electrode potential at which $CO_2$ is first detected (appearance potential). Quantitative kinetic measurements using the carbon-supported catalysts were obtained with the thin-film rotating disk electrode (TF-RDE) method. The $CO_{ad}$ stripping voltammetry clearly indicated that the 500N sample exhibits the lowest degree of alloying, showing a superposition of $Pt_3Sn$ and Pt features, whereas the catalyst consisting entirely of stoichiometric $Pt_3Sn$ cubic phase (E270 sample) exhibits no features characteristic of pure Pt. None of the three carbon-supported Pt–Sn catalysts had the splitting of the C=O stretching band of characteristic of $CO_{ad}$ on $Pt_3Sn(111)$, the surface with the highest specific activity (turnover number) for CO and $H_2$/CO oxidation. All three catalysts had very high levels of activity for $H_2$ oxidation. The mass activity for CO and $H_2$/CO oxidation was proportional to the amount of $Pt_3Sn$ phase in the catalyst. There is no clear evidence that either the PtSn phase or Pt/$SnO_2$ clusters contribute any significant activity for $H_2$/CO or CO oxidation in these catalysts.


*Keywords:* Pt–Sn alloys; CO oxidation; Hydrogen/CO mixtures; IR spectroscopy

## 1. Introduction

Bimetallic alloys are widely used as electrode materials in fuel cells, especially for the electrooxidation of carbon monoxide (CO) and/or hydrogen/carbon monoxide ($H_2$/CO) mixtures. Pt–Sn alloys are one of the most active bimetallic systems (see, for example, Refs. [3–10]). The majority of previous studies of Pt alloy catalysts in fuel cells employed an unsupported polycrystalline form. Our previous studies with $Pt_3Sn(hkl)$ single-crystal electrodes have shown that the electrochemical oxidation of carbon monoxide in acid electrolyte is a structure-sensitive reaction, in which the (111) surface (25 at% Sn) has the highest activity [3,7]. There have been surprisingly few studies of fuel cell reactions with carbon-supported Pt–Sn catalysts. Schmidt et al. [8] used a commercially available carbon-supported Pt–Sn (75 at% Pt) catalyst for the electrooxidation of $H_2$/CO

* Corresponding author.
*E-mail address:* pnross@lbl.gov (P.N. Ross).
[1] Present address: Department of Physical Chemistry I, Technical University of Munich.

0021-9517/$ – see front matter 
doi:10.1016/j.jcat.2005.03.022

mixtures and found very similar activity to the $Pt_3Sn(111)$ and/or (110) surfaces. In contrast to these studies of alloyed Pt and Sn, there are also reports of a promotional effect for $H_2$/CO electrooxidation on nonalloyed $SnO_x$ phase(s) impregnated into carbon-supported Pt [5]. Thus, one should expect very preparation-sensitive activity for carbon-supported Pt–Sn catalysts in this reaction, and to understand this sensitivity it is essential to make a detailed characterization of all phases present, as we have done in Part I [1].

In the present work, we examine the catalytic activity and the relationship of activity to the microstructure of the catalysts. The mass activity (rate per gram of Pt) for the electrooxidation of $H_2$, CO, and $H_2$/CO mixtures is established by the thin-film RDE method. The specific activity (activity per unit area of alloy) or turnover number (activity per active site) is difficult to determine in the Pt–Sn alloy system, however. The usual methods of surface area determination by integration of the charge for oxidation of either adsorbed hydrogen or adsorbed CO cannot be applied, because of strong electronic modification of these states by the Sn [2,3,8]. We present an alternative approach to determining the active site density from the fine features in the vibrational spectra of CO adsorbed on these high-surface-area catalysts and correlating these features with those seen on the $Pt_3Sn(hkl)$ single-crystal surfaces. We also examine the question of the promotional role of $Sn/SnO_2$ atoms, that is, whether Sn has to be present in metallic form alloyed to Pt, and whether the promotional role is a bifunctional or a ligand effect.

## 2. Experimental

### 2.1. High-surface-area catalyst preparation

The Pt–Sn high-surface-area catalysts studied here (samples 500N and 900N) were supplied by the Johnson Matthey Technology Center (Reading, UK), and the third one (denoted E270) by was supplied by E-Tek (Somerset, NJ, USA). The 500N and 900N samples were used with an acetylene black (Shawinigan) carbon support with a Pt/Sn stoichiometry of 1.23:1 and a metal loading of 23 wt%. They were made from the same Pt–$SnO_x$ precursor used previously [5], but differ in the thermal treatment they received to decompose the precursor and promote alloying of the two metals (500 or 900 °C, respectively, in an atmosphere of $N_2$). The E-Tek sample, prepared by a proprietary method, was used with Vulcan XC-72 (Cabot) carbon black, at a Pt/Sn stoichiometry of 3:1, and a metal loading of 20 wt%, with reduction in $H_2$ at 270 °C as the final step in preparation.

### 2.2. Electrochemical measurements

The electrochemical measurements were conducted in a thermostatted standard three-compartment electrochemical cell. A circulating constant-temperature bath (Fisher Isotemp Circulator) maintained the temperature of the electrolyte within ±0.5 °C. The reference electrode was a saturated calomel electrode (SCE) separated by a closed bridge from the reference compartment. All potentials, however, were referenced to the potential of the reversible hydrogen electrode (RHE) at the same temperature (calibrated from the hydrogen oxidation reaction) in the same electrolyte. The preparation of the catalyst layer on the surface of the glassy carbon rotating disk electrode (RDE) has been described previously [11]. In short, the catalyst was dispersed ultrasonically in diluted Nafion solution (Aldrich), and 20 µl of the suspension was pipetted onto a glassy carbon substrate (0.283 $cm^2$ geometrical surface area), leading to a Pt loading of 14 $\mu g_{Pt}/cm^2$. After drying in an Ar atmosphere, the catalyst film is attached to the substrate by a thin (< 0.2 µm) film of recast Nafion. As shown previously, the electrochemical response and the mass transport of the reactants is not influenced by the Nafion thin film [12]. The thus prepared surface was then transferred to the electrochemical cell protected by a drop of ultrapure water and immersed under potential control at 0.05 V in argon-saturated solution, and a cyclic voltammogram was recorded. The upper potential limit was set at 0.5 V versus RHE to avoid Sn dissolution. CO stripping curves were recorded after the surface was saturated with CO for at least 5 min at a potential of 0.05 V and subsequently all CO was removed from the solution by purging with argon for 30 min. Stripping curves are recorded with a scan rate of 10 mV/s, and the upper potential limit was set at 1.0 V to guarantee the complete oxidation of the CO adlayer. In order to measure the continuous electrooxidation of pure $H_2$ or CO ($CO_b$) gas with the RDE, we equilibrated the electrolyte for 5 min with the respective gas while holding the potential at 0.05 V. For the $H_2$/CO mixture, a longer 25-min hold was used to reach the CO equilibrium coverage. Subsequently the potential was scanned positively at a sweep rate of 1 mV/s while the electrode was rotated at 2500 rpm. We expressed the catalytic activity is expressed as mass activity (i.e., $mol/g_{Pt}$) by dividing the current by $nF$ ($F$: Faraday constant; $n$: number of electrons involved in the reaction; $n = 2$ for either $H_2$ or CO oxidation).

### 2.3. Infrared spectroscopy

The detailed catalyst preparation for FTIR spectroscopy of the HSAC is described in a separate paper [13]. In short, the catalyst was dispersed ultrasonically in water, and about 20 µl of the suspension was pipetted onto a heated (∼ 140 °C) gold substrate (0.785 $cm^2$ geometrical surface area), cooled in an argon stream, and rinsed carefully with ultrapure water to remove loosely bound catalyst particles. No further attachment to the substrate was necessary; that is, there was no Nafion film. For the in situ FTIR measurements, a Nicolet Nexus 670 spectrometer was used, which was equipped with a liquid-$N_2$ cooled MCT detector. All IR measurements were performed in a spectroelectrochemical glass cell designed for the external reflection mode. The

cell is coupled at its bottom with a $CaF_2$ prism beveled at 60° from the prism base. The experimental procedure for the IR measurements followed that for the measurement of the polarization curves. Before each experiment the solution was saturated with argon. The electrode was immersed in the electrolyte at a potential of 0.05 V, then CO was introduced into the solution for at least 5 min, and subsequently the sample was pressed against the prism. Starting at a potential of 0.05 V, the potential was scanned at a rate of 5 mV/s in the positive direction while spectra consisting of a single scan were continually recorded. The recording time was thus reduced to ca. 1 s per spectrum. The resolution of the spectra was 4 $cm^{-1}$, and *p*-polarized light was used. Absorbance spectra were calculated as the ratio $-\log(R/R_0)$, where $R$ and $R_0$ are the reflectance values corresponding to the sample and reference spectra, respectively. To obtain the $CO_{ad}$ spectra, the reference spectrum was recorded at 0.80 V, where $CO_{ad}$ is completely oxidized. To follow the production of $CO_2$, we referenced the spectrum recorded at 0.05 V to the spectra recorded at the potentials indicated. The potential in the spectroelectrochemical cell was controlled by a reversible hydrogen electrode (RHE).

## 3. Results and discussion

Before introducing our results for the catalytic activity of the Pt–Sn catalysts, we briefly summarize the basic characterization of the different catalysts presented in the first part of the paper [1].

### 3.1. High-surface-area catalyst characterization

Three different carbon-supported Pt–Sn catalysts were available. The composition, size, distribution, and morphology of the phases present in three different carbon-supported Pt–Sn catalysts were analyzed by high-resolution transmission electron microscopy (HRTEM), microchemical analysis by X-ray emission spectroscopy (EDS), and X-ray diffraction (XRD) [1]. The catalysts had nominal Pt/Sn atomic ratios of 1:1 (500N and 900N samples) and 3:1 (E270 sample). The results showed that the 1:1 catalyst sample heat-treated at 500 °C (500N) contained a Pt-rich $Pt_3Sn$-type cubic phase ($a_0 = 0.3965$ nm) and tetragonal $SnO_2$. The sample from the same precursors heat-treated at 900 °C (900N) consisted of stoichiometric hexagonal PtSn, a nearly stoichiometric $Pt_3Sn$-type cubic phase ($a_0 = 0.3988$ nm), and tetragonal $SnO_2$. Neither pure tin nor pure platinum particles were detected in any of the catalysts. The 3:1 catalyst sample reduced in $H_2$ at 270 °C (E270) was composed entirely of the stoichiometric $Pt_3Sn$ cubic phase ($a_0 = 0.3998$ nm). The $Pt_3Sn$-type particles are predominantly single nanocrystals with mean diameters of ∼ 3–4 nm (E270), ∼ 4 nm (500N), and ∼ 5 nm (900N), and the PtSn particles in the latter sample were larger (taken together, this leads to an average particle size of ∼ 6 nm). For the histograms

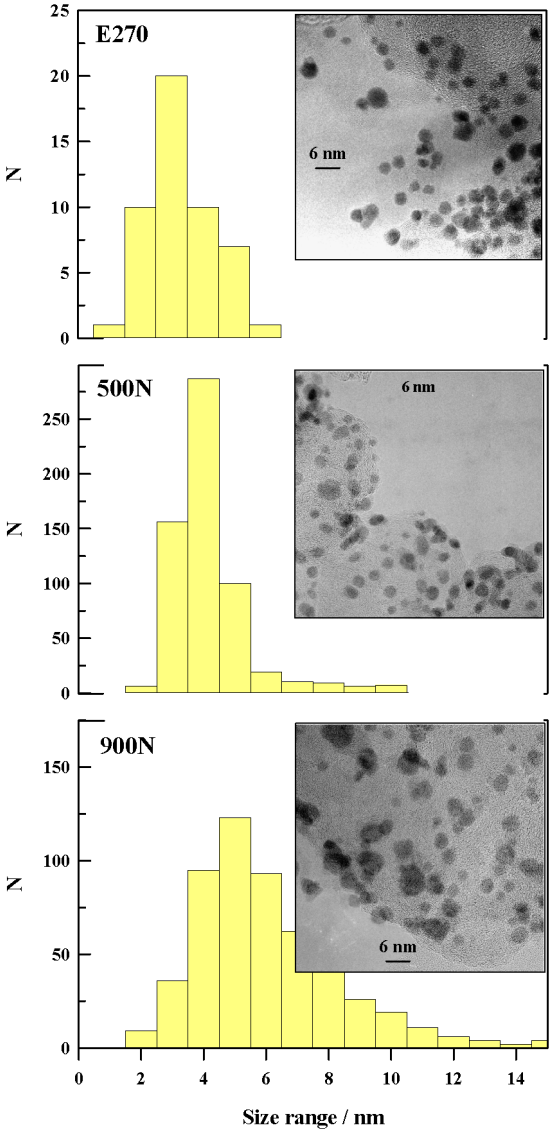


Fig. 1. Typical TEM micrographs of the carbon-supported PtSn high surface area catalysts with the corresponding histograms of the particle size distribution: E270, average particle size about 3–4 nm; 500N average particle size about 4 nm, and 900N average particle size about 6 nm.

of the particle size distribution of the catalysts, see Fig. 1. The $Pt_3Sn$-type particles in the 500N and 900N are generally highly faceted, with {111} and {200} facets, whereas those in the E270 catalyst generally had a smooth spheroidal outline [1]. Whereas the $Pt_3Sn$ particles in the E270 and 900N catalysts were equiaxed, in the 500N catalyst the $Pt_3Sn$ particles had uniquely elongated (e.g., ellipsoidal) shapes. For more details see Ref. [1].

### 3.2. Catalytic activity for CO electrooxidation

The three Pt–Sn catalysts have significantly different Pt–Sn coordinations, and thus one expects significantly different catalytic properties if this coordination is important. In the 500N catalyst, the Pt and $SnO_2$ precursors have only par-

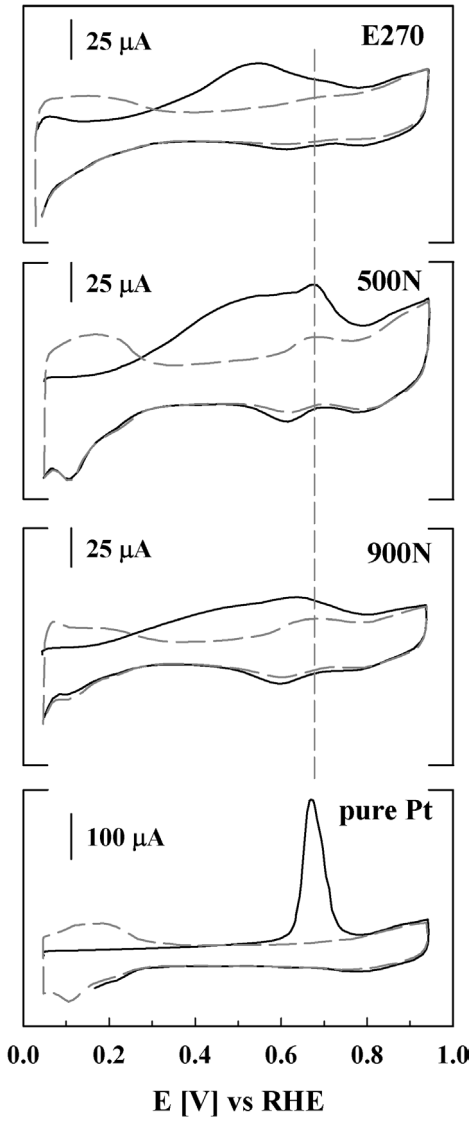


Fig. 2. Comparison of CO stripping curves of a saturated CO adlayer in 0.5 M $H_2SO_4$ solution purged with argon for 30 min at 0.05 V; $T = 60\,^{\circ}C$, scan rate 10 mV/s; dashed curves show second sweep; Pt loading of all catalyst is 14 µg/cm$^2$: E270; 500N; 900N and pure Pt HSAC for comparison.

tially reacted to form a relatively small amount of $Pt_3Sn$-like alloy. All remaining $SnO_2$ particles appear to be closely associated with Pt-like particles, and it would be interesting to determine whether a catalytically synergistic effect comparable to that in $Pt_3Sn$ alloy exists for these $Pt/SnO_2$ clusters. One of the consequences of the incomplete alloying process can be seen in the anodic stripping curves for $CO_{ad}$ in comparison to that for a carbon-supported pure Pt catalyst (HSAC), as shown in Fig. 2. For pure Pt HSAC, the $CO_{ad}$ is oxidized in a relatively sharp stripping peak centered at $\sim 0.7$ V (see Fig. 2). By comparison, on the E270 catalyst, which is composed entirely of $Pt_3Sn$ nanoparticles, $CO_{ad}$ is oxidized over a broad potential region beginning at potentials as low as 0.2 V with a peak at ca. 0.5 V. The $CO_{ad}$ oxidation on the 500N catalyst appears to occur in (at least) two distinct potential regions, one $Pt_3Sn$-like and one Pt-like, consistent with the microstructure of $Pt_3Sn$-like phases and Pt-like phases. It would appear from this result that the clusters of $Pt/SnO_2$ do not have synergistic properties for $CO_{ad}$ oxidation; that is, the Pt behaves like Pt. In agreement with previous results for $Pt_3Sn$ bulk alloy electrodes [7,14], although $CO_{ad}$ oxidation starts at very low potentials, the CO adlayer can be only partially removed at low potentials ($< 0.5$ V), even if several cycles are applied (not shown). To achieve complete $CO_{ad}$ stripping, that is, complete restoration of the charge for hydrogen adsorption/desorption pseudocapacitance, the electrode potential has to be at least 0.9 V, as in Fig. 2. The excursion to this very positive potential, however, causes dissolution of Sn from the surface and thus alters the surface irreversibly, as manifested in a change in the cyclic voltammogram (for more details see [7,14]). Thus determination of the specific activity for Pt–Sn is not possible. For pure Pt the unit area of catalyst, necessary for the determination of the specific activity, can be established either by the $H_{upd}$ (under potential deposited hydrogen) or the CO stripping charge (the turnover frequency (TOF)) is calculated by $\mathrm{TOF} = i/nFN$, where $i$ is the measured current density per unit area, $N$ is the density of active sites, and $n$ is the number of electrons involved in the reaction (for more details see [15]). However, for Pt–Sn catalysts neither method is suitable for establishing either the number of active sites or the metallic area of the catalyst, because on one hand in CO stripping, processes such as Sn dissolution occur parallel to CO oxidation. On the other hand, $H_{upd}$ features are clearly visible only at the electrodes scanned up to 1 V, that is, after there has been some Sn dissolution (see below). Therefore, for our purposes here, the CO stripping curves are used only as a "fingerprint" to detect Pt-like characteristics in the catalysts (note that before the stripping curves were recorded the positive potential limit was 0.5 V).

From Fig. 2 it is obvious that the 500N sample exhibits the most pronounced Pt-like features. By comparison, a sample from the same precursor, treated at a higher temperature (900N), shows a clearly reduced Pt-like $CO_{ad}$ oxidation peak indicating more complete alloying, consistent with the microstructural analysis [1]. The $CO_{ad}$ stripping curve for the 900N is the most complex and appears to be composed of multiple potential regions. Since this is the only catalyst with some stoichiometric PtSn phase, it is possible that one of these multiple regions corresponds to a unique oxidation potential for $CO_{ad}$ on PtSn nanoparticles.

The polarization curves for $H_2$, $H_2$/2% CO, and CO oxidation recorded in the TF-RDE configuration are summarized in Fig. 3. All measurements are performed in 0.5 M $H_2SO_4$ solution at an electrolyte temperature of 60 °C; the catalytic activity is expressed in mass activity, that is, moles reactant (hydrogen and CO) per unit mass of platinum. The polarization curves were recorded at a scan rate of 1 mV/s, at 2500 rpm, whereas the cyclic voltammograms (dashed curves) were recorded without rotation at 50 mV/s in argon-purged solution. The positive potential was limited to 0.5 V

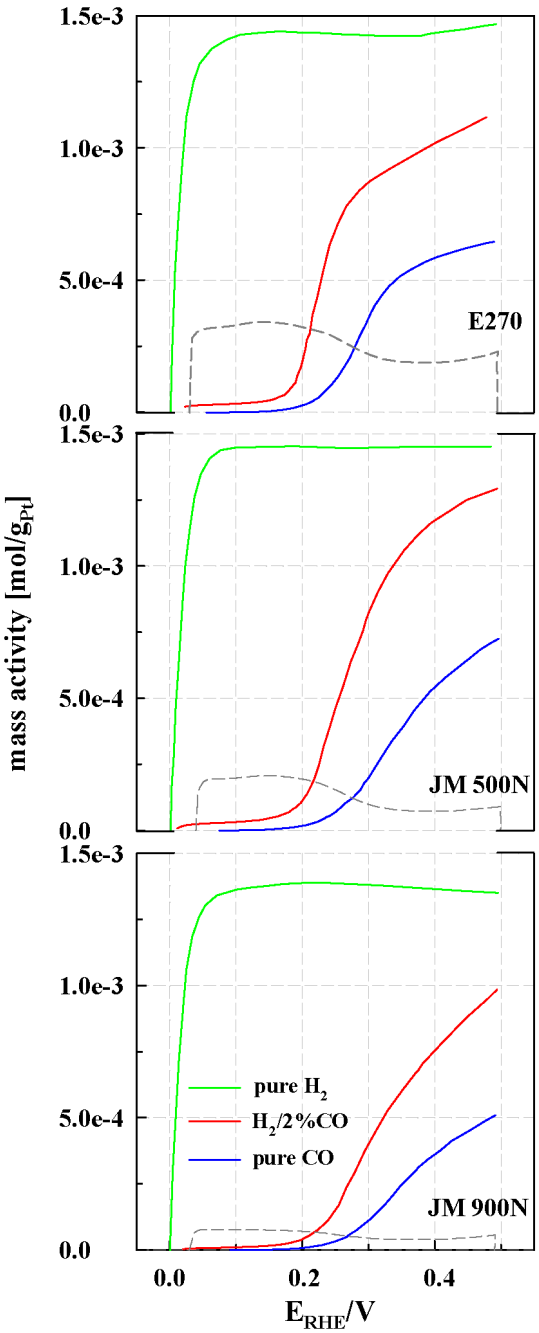


Fig. 3. Polarization curves for different Pt–Sn/C catalysts recorded in 0.5 M $H_2SO_4$ solution saturated with either pure hydrogen, a $H_2$/2% CO mixture, or pure CO; curves are recorded at 60 °C with 1 mV/s and 2500 rpm; dashed curves: CV (a.u.) in argon purged solution at 60 °C, scan rate 50 mV/s.

to avoid Sn dissolution. As shown in Fig. 3, the polarization curves of pure hydrogen are very similar, and no differences in mass activity are clearly seen; that is, all catalysts are extremely active for $H_2$ oxidation. Note, however, that the diffusion-limited current density for the 900N sample is slightly lower than for the other two samples, indicating that the former sample is not completely evenly distributed over the glassy carbon support. In contrast to the hydrogen oxidation reaction, pronounced differences are observed for continuous CO oxidation and the continuous oxidation of a $H_2$/2% CO mixture. As in the $CO_{ad}$ stripping curves, the onset of bulk CO oxidation is observed at approximately 0.2 V on all three catalysts, and consequently at this potential the oxidation of hydrogen starts in the case of the $H_2$/CO mixture. As we have discussed in detail in studies of Pt(*hkl*) single crystals [16,17], in $H_2$/CO mixtures $H_2$ acts like a "current multiplier" for the CO oxidation current; that is, if a Pt–$CO_{ad}$ site is freed because of CO oxidation, then hydrogen oxidation starts at this site at a much higher rate (current). Consequently, the onset of CO oxidation is easier to detect in $H_2$/CO mixtures. For the Pt–Sn catalysts the order for mass activity is E270 > 500N > 900N. At 0.3 V, the CO oxidation rate is about two times higher for 500N versus 900N, and about two times higher for E270 versus 500N. Note that with a pure Pt HSAC, there is no measurable current for CO or $H_2$/CO oxidation at any potential below 0.5 V.

In our study of the $Pt_3Sn$(*hkl*) surfaces, the two surfaces with 25 at% Sn, annealed $Pt_3Sn$(111), and lightly sputtered $Pt_3Sn$(110), had superior activity compared with the sample with 50 at% Sn on the surface (annealed $Pt_3Sn$(110)) [2,3]. Therefore the low catalytic activity of the 900N sample is most likely due to the higher content surface concentration of Sn as a consequence of the high annealing temperature (900 °C). Our analysis in Part I [1] indeed showed that this sample (900N) consists in part of stoichiometric PtSn particles. Furthermore, it may well be that even the stoichiometric $Pt_3Sn$ particles have a 50% Sn surface concentration, depending on the detailed surface structure of these particles. An observation supporting this supposition is the fact that in the cyclic voltammogram of the 900N sample (Fig. 3) $H_{upd}$ features are almost absent, as is also the case for the annealed $Pt_3Sn$(110) surface [2]. Note that if the potential is scanned up to 1 V, Sn dissolves and subsequently $H_{upd}$ can be seen (see Fig. 2).

By contrast, the comparably mild preparation temperatures (270 °C) for the E270 sample most likely prevent such a segregation of Sn, and from the above results (Fig. 3) stoichiometric $Pt_3Sn$ can be identified as the most active phase. Another interesting result is the fact that the 500N sample is quite active, that is, it has a mass activity similar to that of the E270 sample, although in the CO stripping curves the former showed the most pronounced "Pt-like" behavior. The analysis in Part I showed that the 500N sample consists of a Pt-rich $Pt_3Sn$-type cubic phase and tetragonal $SnO_2$; the $SnO_2$ particles in the sample appear to be closely associated with Pt-like particles, that is, unalloyed Pt. A catalytically synergistic interaction between unalloyed Pt and $SnO_2$ might therefore occur in the 500N catalyst, as implied by the reported promotional effect of nonalloyed $SnO_x$ phase(s) impregnated in carbon-supported Pt [5]. Here the relatively high mass activity of the 500N sample at very low potential (i.e., below 0.3 V) further supports that proposition. In the potential region between the onset of measurable current with pure CO, near 0.2 V, and 0.3 V where the current be-

comes significant, the current ratio between 500N and the E270 exceeds the factor of 2 difference in $Pt_3Sn$ content in the two catalysts.

### 3.3. FTIR measurements

Before describing the FTIR spectra of CO adsorbed on Pt–Sn nanoparticles, we briefly summarize our previous FTIR results of CO adsorption on $Pt_3Sn(hkl)$ single-crystal electrodes [2,3]. As we reviewed in the Introduction, the electrochemical oxidation of carbon monoxide is a strongly structure-sensitive reaction, for which the $Pt_3Sn(111)$ surface (25 at% Sn) has the highest activity [3,7]. The high activity on this surface is linked to the formation of a compressed CO adlayer associated with the observation of a splitting of the C–O stretching frequency of a-top bonded CO. By comparison, on the lightly sputtered and the annealed $Pt_3Sn(110)$ surface (25 and 50 at% Sn, respectively), no compressed adlayer is formed and only a single peak can be observed in the spectra. On these surfaces the oxidation of solution-phase CO compared with $Pt_3Sn(111)$ is shifted by $\sim 100$ and $\sim 200$ mV, respectively, to more *positive* potentials. The C–O stretching frequency, however, is not affected by the surface concentration of Sn [2]. For more details see Refs. [2,3].

A series of representative FTIR spectra for Pt–Sn nanoparticles (E270 sample) obtained in CO-saturated 0.5 M $H_2SO_4$ is shown in Fig. 4. The spectra consist of a main band around 2060 $cm^{-1}$ and a smaller band around 1880 $cm^{-1}$, which can be assigned, respectively, to a-top and bridge bonded CO on the Pt sites [18]. The absorption bands are broader than spectra obtained on $Pt_3Sn(hkl)$ bulk electrodes [2,3] but similar to the respective bands for bands typical for carbon-supported pure Pt catalyst [13]. The most important result displayed in Fig. 4 is the fact that no peak splitting of the a-top CO can be observed on the E270 sample (or on either of the two other Pt–Sn catalysts). Consequently, none of the Pt–Sn HSAC catalysts indicates the formation of the compressed CO adlayer characteristic for the $Pt_3Sn(111)$ electrode [3]. It would appear that the formation of this compressed adlayer requires larger $Pt_3Sn(111)$ facets that are formed on the nanoparticles in these carbon-supported catalysts.

In order to compare the onset of CO oxidation on the different Pt–Sn catalysts in a controlled way, we monitored $CO_2$ production while scanning the potential with a fixed scan rate (5 mV/s), as in the electrochemical measurements, while continuously recording spectra [19]. The results of these measurements on the Pt–Sn HSAC are summarized in Fig. 5, whereas in Fig. 6 results obtained for a pure Pt HSAC control sample (E-Tek; metal loading 30 wt%) are displayed separately reduce the complexity of the figures. The insets in the figures show the (first) spectrum from the respective series recorded at 0.05 V. By analyzing the potential-dependent peak area of $CO_2$ in Fig. 5, one can see that CO oxidation starts at the same potential on all Pt–Sn alloys, that is, under these experimental conditions at $\sim 0.30$ V. Interestingly, on the Pt–Sn HSAC the onset of $CO_2$ production is shifted by only $\sim 50$ mV relative to the pure Pt HSAC (see Fig. 6). There are two phenomena that cause this shift to be smaller than it is in practice, that is, in a fuel cell anode. One is the integrating nature of the measurement of $CO_2$ in solution in the thin-layer geometry of the IR cell; that is, the rate of $CO_2$ production (the current) is proportional to the derivative of the $CO_2$ intensity, and the other is the unsteady, fundamentally time-dependent nature of CO oxidation on pure Pt surfaces, as we have discussed in detail previously [16,17,20]. The former phenomenon is illustrated by noting that when the potential is held for a longer time (> 1 min), $CO_2$ formation can be observed on the Pt–Sn nanoparticles at potentials as low as 100 mV. However, in contrast to Pt–Sn nanoparticles, on pure Pt nanoparticles no $CO_2$ can be observed when the potential is held at 100 mV for any extended period. The latter phenomenon is seen in Figs. 5 and 6; in contrast to Pt–Sn, the potential-dependent plot of the $CO_2$ peak area for Pt shows two regions with different slopes. At

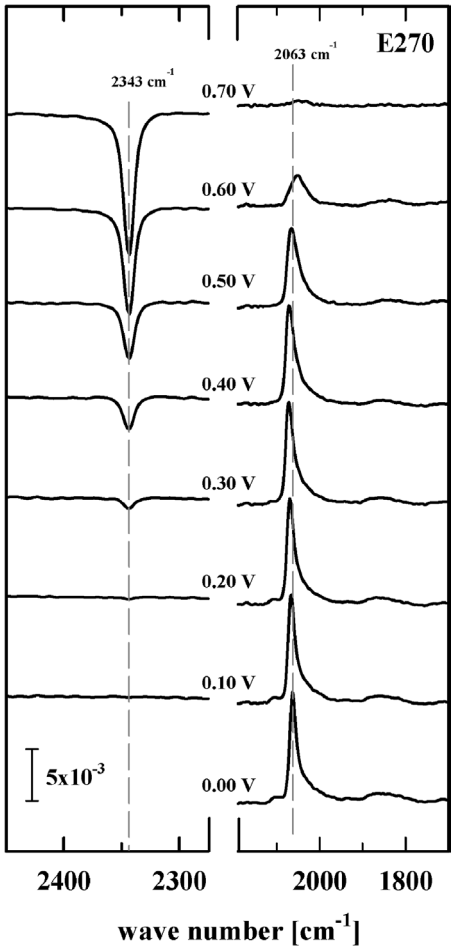


Fig. 4. Series of potential-dependent FTIR spectra from the E270 sample recorded in CO saturated 0.5 M $H_2SO_4$ solution; the respective electrode potential is indicated; for each spectra 50 scans were co-added, resulting in a recording time of ca. 25 s. The left column of spectra represents evolution of $CO_2$, while corresponding CO spectra is given in the right column.

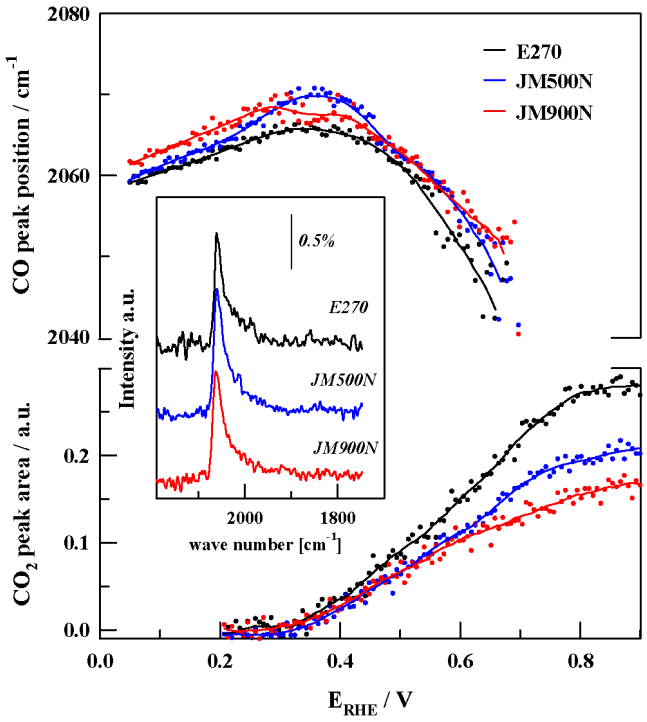


Fig. 5. Potential-dependent band position and integrated intensities of the $CO_2$ bands of series of potential-dependent FTIR spectra of the different PtSn HSAC; all spectra are recorded in CO saturated 0.5 M $H_2SO_4$ solution while scanning the potential with 5 mV/s starting at 50 mV; each spectra consists of 1 interferometer scan; the insert shows the first $CO_{ad}$ spectrum of each catalyst.

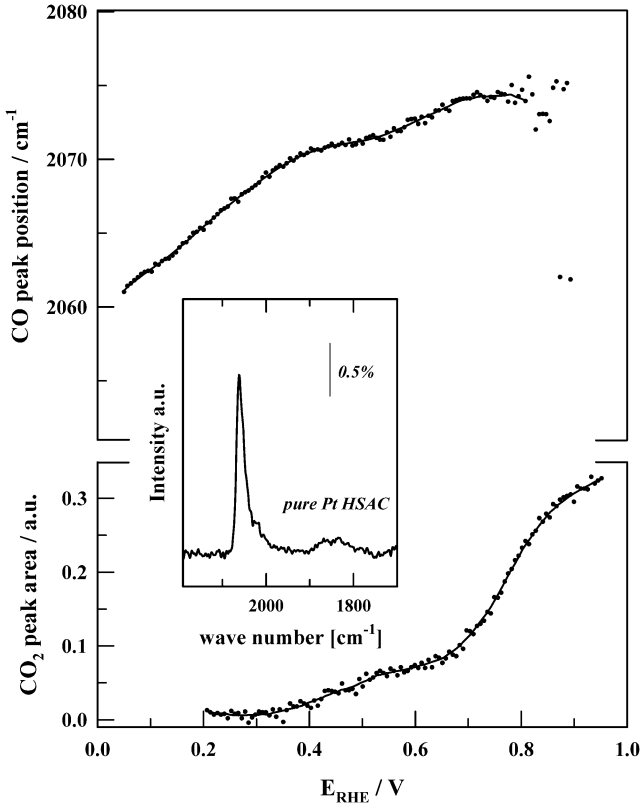


Fig. 6. For comparison potential-dependent band position and integrated intensities of the $CO_2$ bands of a series of potential-dependent FTIR spectra of a pure Pt HSAC; all spectra are recorded in CO saturated 0.5 M $H_2SO_4$ solution while scanning the potential with 5 mV/s starting at 50 mV; each spectra consists of 1 interferometer scan; the insert shows the first spectrum.

low potentials for Pt ($0.3 < E < 0.65$ V) the increase in the peak area with potential (or time) is much smaller than at high potentials, that is, at $E > 0.65$ V. In the low-potential region (pre-ignition region), the CO oxidation reaction on bulk Pt surfaces is time-dependent and eventually decreases (to near zero) when the potential is held constant [20]. Only above 0.7 V, where a sharp increase in the $CO_2$ peak area is observed with the Pt HSAC catalyst, is there a sustained high rate of CO oxidation, leading us to characterize the potential of 0.7 V and above as the ignition potential [20]. By contrast, the $CO_2$ peak area with the Pt–Sn catalysts in Fig. 5 shows a constant increase with the applied potential, and the oxidation current remains steady if the potential is held at any potential above ca. 0.4 V.

More details about the promotional effect of Sn are provided by the potential dependence of the C–O vibrational frequency. At low potentials, the C–O stretching frequency is the same on the Pt–Sn and pure Pt HSAC; for example, at 50 mV the C–O frequency of a-top CO is about $2061 \pm 4\ \mathrm{cm}^{-1}$ on all surfaces. By this measure, there is no unambiguous weakening in the strength of the CO backbonding from the intermetallic bond between Pt and Sn (i.e., the ligand effect). The same linear shift of the C–O stretch frequency with the applied potential, the so-called Stark-shift [21,22], occurs with both Pt–Sn and pure Pt HSAC at potentials below ca. 0.4 V. However, significant differences in the dependence of $\nu_{CO}$ vs $E$ between Pt and Pt–Sn do appear at potentials above 0.4 V, where sustained oxidation of CO occurs on the Pt–Sn catalysts. The current interpretation of the transition to a negative Stark tuning slope, $\mathrm{d}\nu/\mathrm{d}E$, on Pt surfaces is that above the ignition potential, the steady-state coverage by $CO_{ad}$ begins to decrease sharply with increasing potential, and the dipole–dipole coupling is thereby reduced, (down)shifting the frequency. Because the coverage decreases rapidly with potential in this region, the down-shift from reduced dipole coupling exceeds the up-shift from the Stark effect, leading to a net negative $\mathrm{d}\nu/\mathrm{d}E$. What complicates the detailed analysis of this process on pure Pt surfaces is the clustering of the remaining $CO_{ad}$ molecules as $OH_{ad}$ nucleates on the surface, which maintains stronger local dipole–dipole coupling than would be expected with randomly dispersed $CO_{ad}$. Pt alloys like Pt–Ru and, here, Pt–Sn show fundamentally different behavior with respect to this phenomenon, where the Stark tuning slope becomes negative concomitantly with the detection of $CO_2$ dissolved in solution. Most probably this fundamental difference in the negative Stark tuning between pure Pt surfaces and the Pt alloy surfaces is due to the very different way in which $OH_{ad}$ nucleates on the surfaces. In the case of the alloys, preferentially on the admetal sites, which are either randomly (Ru) or periodically (Sn) distributed in the surface, but in pure Pt

surfaces the $OH_{ad}$ follows a classical nucleation and growth pattern. The negative Stark tuning slopes above 0.4 V on all three Pt–Sn HSAC are remarkably similar. This observation implies that the active sites in the three catalysts are essentially the same, and that the differences in the overall rates are due primarily to the variation in the surface concentration of active sites in the catalysts. Since the E270 catalyst is the most active, and has only the $Pt_3Sn$ phase present, this would in turn imply that the sites on the $Pt_3Sn$ surface are the most active sites, which is in accordance to the discussion and results related to $Pt_3Sn(hkl)$ properties described in Section 3.2. There is no clear evidence that either the PtSn phase or $Pt/SnO_2$ clusters contribute any significant activity for $H_2$/CO or CO oxidation in these catalysts.

### 3.4. Reaction mechanism

The bifunctional reaction mechanism of CO oxidation on Pt alloys is usually described as a Langmuir–Hinshelwood (L-H)-type reaction, where the alloying component, here Sn, preferentially adsorbs oxygenated species (simply represented as $OH_{ad}$) from dissociation of water. The respective elementary steps are as follows:

$$Pt_* + CO_{diss.} = Pt\text{–}CO_{ad}, \quad (1)$$

$$Sn_* + H_2O = Sn\text{–}OH_{ad} + H^+ + e^-, \quad (2a)$$

$$SnO_{2*} + H_2O = SnO_2\text{–}OH_{ad} + H^+ + e^-, \quad (2b)$$

$$Pt\text{–}CO_{ad} + Sn\text{–}OH_{ad} = CO_2 + H^+ + e^-, \quad (3a)$$

$$Pt\text{–}CO_{ad} + SnO_2\text{–}OH_{ad} = CO_2 + H^+ + e^-. \quad (3b)$$

The presence of Sn in the surface thus allows for the continuous oxidation of the CO at a potential where $OH_{ad}$ does not form on Pt. The relatively large amounts of unalloyed $SnO_2$ on two of the catalysts studied here suggest that, as was proposed previously [5], not only Sn atoms but also $SnO_2$ (or Sn hydro-oxides) adjacent to Pt may provide a bifunctional effect as well, as shown by reaction schemes (3a) and (3b). Support for this supposition may also be found in the gas-phase oxidation of CO at room temperature on Pt supported on $SnO_2$ [23,24]. We recall that the chemical nature of the oxygenated species is still unknown, that is, it can be either $OH_{ad}$ or oxide. However, the rate of CO oxidation at low potential appears to scale with the amount of $Pt_3Sn$ phase present in the catalyst, implying that reaction (3b) does not contribute in any significant way to the total activity of these Pt–Sn catalysts.

In addition to the bifunctional effect, some theories have proposed a ligand effect [25,26], whereby the Sn lowers the adsorption energy of $CO_{ad}$ on neighboring Pt atoms, thus increasing the rate of $CO_{ad}$ surface diffusion and increasing the collision frequency with $OH_{ad}$. However, we could not find any support for the ligand effect based on our FTIR results. Although the exact nature of the oxygenated species associated with the active surface is not known, the promotional effect of Sn in different Pt–Sn catalysts seems to be simply determined primarily by the formation of reactive OH species at a much lower potential than on pure Pt surfaces.

## 4. Conclusions

The catalytic activity of three different carbon-supported Pt–Sn catalysts toward the anodic oxidation of hydrogen, carbon monoxide, and $H_2$/CO mixtures is analyzed. Two of the catalysts had nominal Pt/Sn atomic ratios of 1:1 (500N and 900N samples), whereas one sample had an atomic ratio of 3:1 (E270 sample). The characterization in Part I of the paper showed that the E270 sample was composed entirely of the stoichiometric $Pt_3Sn$ fcc alloy, with the particles predominantly consisting of single nanocrystals with mean diameters of $\sim$ 3–4 nm. By contrast, the 1:1 catalyst samples possibly contained some pure Pt, a Pt-rich $Pt_3Sn$-type cubic phase, tetragonal $SnO_2$ (500N), or stoichiometric hexagonal PtSn, a nearly stoichiometric $Pt_3Sn$-type cubic phase, and tetragonal $SnO_2$ (900N). The mean size of the $Pt_3Sn$-type particles in the latter samples is comparable to that in the E270 sample, $\sim$ 4 and $\sim$ 5 nm for 500N and 900N, respectively, whereas the PtSn particles of the 900N sample are larger. These structural differences lead to different properties for CO stripping and for the electrooxidation of pure CO and a $H_2$/CO mixture. In the CO stripping experiments all Pt–Sn catalysts exhibited CO oxidation at low potentials (0.20 V). The sample that had the least alloying during preparation (500N) exhibited the most pronounced “Pt-like” features. For the continuous oxidation of CO and $H_2$/CO mixtures the E270 sample showed the highest mass activity, followed by the 500N and the 900N samples.

Vibrational spectroscopy of adsorbed CO by in situ FTIR showed that none of the Pt–Sn catalysted exhibits the peak splitting in the C–O stretching of a-top bonded CO unique to the CO adlayer formed on a highly reactive $Pt_3Sn(111)$ surface. Analysis of the potential-dependent CO coverage on the active Pt sites and the potential-dependent C–O stretching frequencies shows very similar behavior for all three catalysts. Based on the band positions, there was no evidence of a ligand effect, that is, increased back-bonding. The promotional effect of Sn in different Pt–Sn catalysts seems to be simply determined primarily by the formation of reactive OH species at a much lower potential than on pure Pt surfaces, that is, the bifunctional effect. The most active sites for CO oxidation (at low potentials) are most probably pairs of Pt–Sn atoms in the $Pt_3Sn$ alloy surface.

## Acknowledgments

This work was supported by the Director, Office of Science, Office of Basic Energy Sciences, Division of Materials Sciences, U.S. Department of Energy, under contract DE-AC03-76SF00098. We thank Dr. David Thompsett from the

Johnson Matthey Technology Center and E-Tek Corporation for supplying the Pt–Sn catalyst samples. M.A. is grateful for a Feodor Lynen fellowship from the German Alexander von Humboldt foundation. K.M. acknowledges the Austrian BMBWK for a scholarship.

## References

[1] V. Radmilovic, T.J. Richardson, S.J. Chen, P.N. Ross Jr., J. Catal. 232 (2005) 199–209.
[2] V. Stamenkovic, M. Arenz, B.B. Blizanac, K.J.J. Mayrhofer, P.N. Ross, N.M. Markovic, Surf. Sci. 576 (2005) 145–157.
[3] V.R. Stamenkovic, M. Arenz, C.A. Lucas, M.E. Gallagher, P.N. Ross, N.M. Markovic, J. Am. Chem. Soc. 125 (2003) 2736–2745.
[4] H.A. Gasteiger, N.M. Markovic, P.N. Ross, J. Phys. Chem. 99 (1995) 8945–8949.
[5] E.M. Crabb, R. Marshall, D. Thompsett, J. Electrochem. Soc. 147 (2000) 4440–4447.
[6] A.C. Boucher, N. Alonso-Vante, F. Dassenoy, W. Vogel, Langmuir 19 (2003) 10885–10891.
[7] H.A. Gasteiger, N.M. Markovic, P.N. Ross, Catal. Lett. 36 (1996) 1–8.
[8] T.J. Schmidt, H.A. Gasteiger, R.J. Behm, J. New Mater. Electrochem. Syst. 2 (1999) 27–32.
[9] S. Tillmann, G. Samjeske, K.A. Friedrich, H. Baltruschat, Electrochim. Acta 49 (2003) 73–83.
[10] B.E. Hayden, M.E. Rendall, O. South, J. Am. Chem. Soc. 125 (2003) 7738–7742.
[11] T.J. Schmidt, H.A. Gasteiger, G.D. Stab, P.M. Urban, D.M. Kolb, R.J. Behm, J. Electrochem. Soc. 145 (1998) 2354–2358.
[12] T.J. Schmidt, H.A. Gasteiger, R.J. Behm, J. Electrochem. Soc. 146 (1999) 1296–1304.
[13] V. Stamenkovic, M. Arenz, P.N. Ross Jr., N.M. Markovic, J. Phys. Chem. B (2004), submitted for publication.
[14] K. Wang, H.A. Gasteiger, N.M. Markovic, P.N. Ross, Electrochim. Acta 41 (1996) 2587–2593.
[15] N.M. Markovic, P.N. Ross, CatTech 4 (2000) 110–126.
[16] N.M. Markovic, B.N. Grgur, C.A. Lucas, P.N. Ross, J. Phys. Chem. B 103 (1999) 487–495.
[17] N.M. Markovic, C.A. Lucas, B.N. Grgur, P.N. Ross, J. Phys. Chem. B 103 (1999) 9616–9623.
[18] S.C. Chang, M.J. Weaver, Surf. Sci. 238 (1990) 142–162.
[19] V. Stamenkovic, K.C. Chou, G.A. Somorjai, P.N. Ross Jr., N.M. Markovic, J. Phys. Chem. B 109 (2005) 678–680.
[20] N.M. Markovic, J. Ross, Surf. Sci. Rep. 45 (2002) 117–229.
[21] D.M. Bishop, J. Chem. Phys. 98 (1993) 3179–3184.
[22] D.K. Lambert, Electrochim. Acta 41 (1996) 623–630.
[23] S.D. Gardner, G.B. Hoflund, B.T. Upchurch, D.R. Schryer, E.J. Kielin, J. Schryer, J. Catal. 129 (1991) 114–120.
[24] D.S. Stark, M.R. Harris, J. Phys. E Sci. Instrum. 16 (1983) 492–496.
[25] T.E. Shubina, M.T.M. Koper, Electrochim. Acta 47 (2002) 3621–3628.
[26] P. Liu, A. Logadottir, J.K. Norskov, Electrochim. Acta 48 (2003) 3731–3742.